ISSN 1990-7931, Russian Journal of Physical Chemistry B, 2025, Vol. 19, No. 3, pp. 688–700. © Pleiades Publishing, Ltd., 2025.

CHEMICAL PHYSICS OF NANOMATERIALS

Comparison between Sodium or Potassium-Ion Batteries and Lithium-Ion Counterparts for Energy-Saving: A Physico-Chemical Study by Density Functional Theory

F. Mollaamin[a], * and M. Monajjemi[b]

[a] *Department of Biomedical Engineering, Faculty of Engineering and Architecture, Kastamonu University, Kastamonu, Turkey*
[b] *Department of Chemical Engineering, Central Tehran Branch, Islamic Azad University, Tehran, Iran*
**e-mail: fmollaamin@kastamonu.edu.tr*

Received December 22, 2024; revised January 17, 2025; accepted January 20, 2025

Abstract—As the incremental deficiency of Li resources, it is significant and instant to supersede Li with other earth-abundant elements for electrochemical energy storage devices. While lithium-ion batteries (LIBs) have their difficulties, the demand to improve beyond-lithium batteries goes beyond the issues of sustainability and safety. Accordingly, Na/K-atom energy storage devices, including rechargeable batteries and ionic capacitors with similar energy storage mechanisms to Li-ion devices, have attracted widespread concerns due to the abundant reserves of Na/K and low cost. Therefore, in this article, it has been evaluated the promising alternative alkali metals of sodium-ion and potassium-ion, batteries. A comprehensive investigation on hydrogen grabbing by Li_2[SnO–SiO], Na_2[SnO–SiO] or K_2[SnO–SiO] was carried out including using DFT computations at the "CAM–B3LYP–D3/6-311+G (*d*,*p*)" level of theory. The hypothesis of the hydrogen adsorption phenomenon was confirmed by density distributions of CDD, TDOS, and ELF for nanoclusters of Li_2[SnO–SiO]–$2H_2$, Na_2[SnO–SiO]–$2H_2$ or K_2[SnO–SiO]–$2H_2$. The fluctuation in charge density values demonstrates that the electronic densities were mainly located in the boundary of adsorbate/adsorbent atoms during the adsorption status. As the advantages of lithium, sodium or potassium over Sn/ Si possess its higher electron and hole motion, allowing lithium, sodium or potassium instruments to operate at higher frequencies than Sn/Si instruments. Among these, sodium-ion batteries seem to show the most promise in terms of initial capacity.

Keywords: sodium or potassium battery, density of states, charge distribution, materials modeling, hydrogen adsorption, energy storage

DOI: 10.1134/S1990793125700319

1. INTRODUCTION

Rechargeable lithium-ion batteries (LIBs) and lithium-ion capacitors have dominated the vast market of electrochemical energy storage devices involving laptops, communication, consumer electronics, and electric vehicles due to their great energy density and stable cycling performance. Although lithium-ion batteries have become available in the current technology perspective through their high energy density, they face serious discussions in terms of safety and sustainability. With the enhancing global request for energy, there is an essential need for alternative efficient energy storage systems. This is driving research into non-lithium battery systems. This paper presents a comprehensive research on non-lithium battery technologies, specifically sodium-ion and potassium-ion batteries [1–10].

Along with the sodium ion, potassium-ion is the prime chemistry replacement candidate for lithium-ion batteries. The potassium-ion has certain advantages over similar lithium-ion such as: the cell design is simple, and both the material and the fabrication procedures are cheaper. The key advantage is the abundance and low cost of potassium in comparison with lithium, which makes potassium batteries a promising candidate for large scale batteries such as household energy storage and electric vehicles. Another advantage of a potassium-ion battery over a lithium-ion battery is potentially faster charging [11–20].

Recently, Si-, Ge- or Sn-carbide nanostructures have been suggested as engaged H-grabbing compounds [14–16]. Since the polarizability of silicon is more than carbon, it is supposed that Si–C/Si nanosheet might attach to compositions more strongly in comparison to the net carbon nano-surfaces [21–31]. It was presented with a novel semiconducting alloy, silicon-tin (SiSn), as channel material for complementary metal oxide semiconductor (CMOS) circuit applications [32].

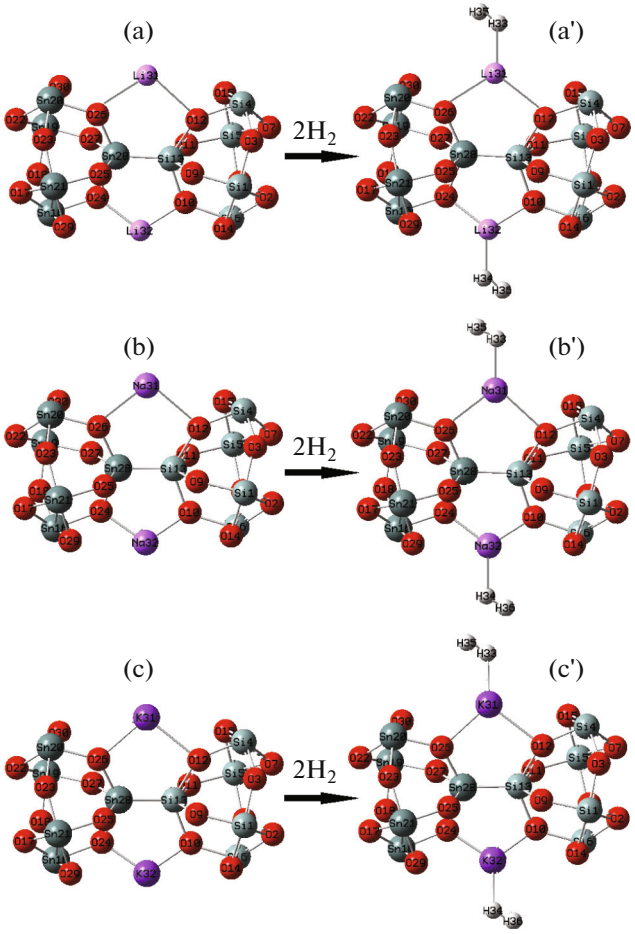

Fig. 1. Adsorption of hydrogen by (a) $Li_2[SnO–SiO]$, to (b) $Na_2[SnO–SiO]$, (c) $K_2[SnO–SiO]$ towards formation of (a') $Li_2[SnO–SiO]–2H_2$, (b') $Na_2[SnO–SiO]–2H_2$, and (c') $K_2[SnO–SiO]–2H_2$.

Nanomaterials with remarkable specific structures indicate promising applications in the field of energy storage, electrocatalysis, and fuel cells [33–41]. In our previous works, the investigation of energy storage in fuel cells through hydrogen adsorption has been accomplished using DFT calculations through different nanomaterials consisting of silicon/germanium/tin/lead nano-carbides [42], magnesium-aluminum alloy [43] and aluminum/carbon/silicon doping boron nitride nanocage [44].

Currently, the present research aims to explore the possibility of using $Li_2[SnO–SiO]$, $Na_2[SnO–SiO]$ or $K_2[SnO–SiO]$ nanocluster for hydrogen storage by employing first-principles calculations. We have analyzed the structural and electronic properties of $Li_2[SnO–SiO]$, $Na_2[SnO–SiO]$ or $K_2[SnO–SiO]$ nanocluster and hydrogen-adsorbed nanoclusters of $Li_2[SnO–SiO]–2H_2$, $Na_2[SnO–SiO]–2H_2$ or $K_2[SnO–SiO]–2H_2$ using state-of-the-art computational techniques. In this work, considering that the physicochemical and electrochemical features of electrolytes play a critical role in the device performance, we have elaborated the advanced analysis and characterization technologies of the electrolytes involving structure evaluation and stability assessment through theoretical approaches.

2. THEORY, MATERIALS AND COMPUTATION

The aim of this study is to hydrogen adsorption by using alkali metals-based nanoclusters of $Li_2[SnO–SiO]/Li_2[SnO–SiO]–2H_2$, $Na_2[SnO–SiO]/Na_2[SnO–SiO]–2H_2$ or $K_2[SnO–SiO]/K_2[SnO–SiO]–2H_2$ (Figs. 1a, 1a', 1b, 1b', 1c, 1c') which can increase the hydrogen storage in cell batteries, transistors or other semiconductors. In our research, the calculations have been done by CAM–B3LYP–D3/EPR–3 level of theory. A new hybrid exchange–correlation functional named CAM–B3LYP is proposed. It combines the hybrid qualities of B3LYP and the long-range correction [45].

Figures 1a, 1a', 1b, 1b', 1c, 1c') shows the process of hydrogen adsorption by $Li_2[SnO–SiO]$, $Na_2[SnO–SiO]$ or $K_2[SnO–SiO]$ nanocluster and hydrogen-adsorbed nanoclusters of $Li_2[SnO–SiO]–2H_2$, $Na_2[SnO–SiO]–2H_2$ or $K_2[SnO–SiO]–2H_2$. The Bader charge analysis [46, 47] was discussed during trapping of hydrogen atoms by $Li_2[SnO–SiO]$, $Na_2[SnO–SiO]$ or $K_2[SnO–SiO]$ nanoclusters (Figs. 1a, 1a', 1b, 1b', 1c, 1c')). The rigid potential energy surface using density functional theory [48–61] was performed due to Gaussian 16 revision C.01 program package [62] and GaussView 6.1 [63]. The coordination input for hydrogen grabbing by $Li_2[SiO–SnO]$, $Na_2[SiO–SnO]$, and $K_2[SiO–SnO]$ applied LANL2DZ and 6-311+G (*d*,*p*) basis sets with multiplicity = 1.

3. RESULTS AND DISCUSSION

3.1. Charge Density Differences Analysis

The amounts of charge density differences (CDD) are measured by considering isolated atoms or noninteracting ones. The mentioned approximation can be the lightest to use because the superposition value may be received from the primary status of the self-consistency cycle in the code that carries out the density functional theory (Figs. 2a, 2a', 2b, 2b', 2c, 2c') [64].

In Fig. 2a, Li_2 [SnO–SiO] cluster with the fluctuation in the region around –12 to +6 Bohr forms the nanocluster of $Li_2[SnO–SiO]–2H_2$ (Fig. 2a') in the area around –12 to +3 Bohr. Furthermore, the atoms of O2, O3, O7–O12, O14, O15, O17, O18, O22–O27, O29, O30 from Na_2 [SnO–SiO] (Fig 2b) have shown the fluctuation around –12 to +4 Bohr towards formation of $Na_2[SnO–SiO]–2H_2$ through hydrogen adsorption (Fig. 2b'). In addition, $K_2[SnO–SiO]$ cluster with the fluctuation in the region around –12 to

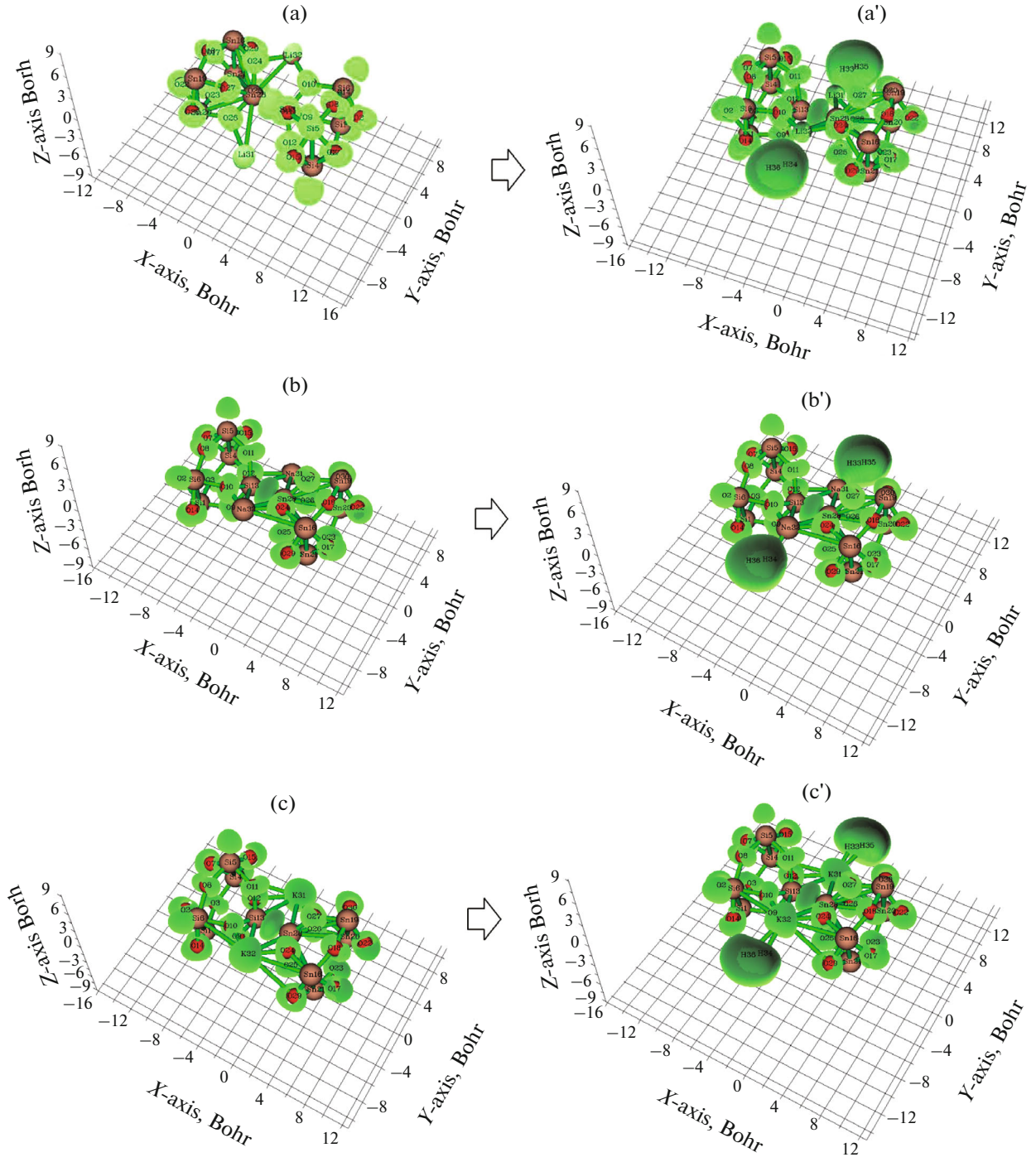

Fig. 2. CDD graphs for (a) $Li_2[SnO–SiO]$, (a') $Li_2[SnO–SiO]–2H_2$, (b) $Na_2[SnO–SiO]$, (b') $Na_2[SnO–SiO]–2H_2$, (c) $K_2[SnO–SiO]$, and (c') $K_2[SnO–SiO]–2H_2$ nanoclusters.

+4 Bohr (Fig. 2c) forms the nanocluster of $K_2[SnO–SiO]–2H_2$ during hydrogen grabbing (Fig. 2c') in the same range of area around −12 to +4 Bohr. Atomic charge was discussed during trapping of hydrogens by $Li_2[SnO–SiO]$, $Na_2[SnO–SiO]$ or $K_2[SnO–SiO]$ nanoclusters towards formation of $Li_2[SnO–SiO]–2H_2$, $Na_2[SnO–SiO]–2H_2$ or $K_2[SnO–SiO]–2H_2$, respectively (Table 1).

The atomic charge of Si, Sn, O, and alkali metals of Li, Na, K and hydrogen atoms absorbed on $Li_2[SnO–SiO]$, $Na_2[SnO–SiO]$ or $K_2[SnO–SiO]$ nanoclusters have been measured. The values detect that with add-

Table 1. The atomic charge (Q/coulomb) for the atomic charge (Q/coulomb) for Li_2[SnO–SiO], Li_2[SnO–SiO]–$2H_2$, Na_2[SnO–SiO], Na_2[SnO–SiO]–$2H_2$, K_2[SnO–SiO] nanoclusters, and K_2[SnO–SiO]–$2H_2$ nanoclusters

Li_2[SnO–SiO]		Li_2[SnO–SiO]–$2H_2$		Na_2[SnO–SiO]		Na_2[SnO–SiO]–$2H_2$		K_2[SnO–SiO]		K_2[SnO–SiO]–$2H_2$	
atom	charge	atom	charge	atom	charge	atom	charge	atom	charge	atom	charge
Si1	1.45	Si1	1.45	Si1	1.46	Si1	1.46	Si1	1.46	Si1	1.45
O2	–0.63	O2	–0.63	O2	–0.63	O2	–0.63	O2	–0.63	O2	–0.70
O3	–0.83	O3	–0.83	O3	–0.83	O3	–0.83	O3	–0.83	O3	–0.83
Si4	1.41	Si4	1.41	Si4	1.40	Si4	1.40	Si4	1.40	Si4	1.41
Si5	1.43	Si5	1.43	Si5	1.44	Si5	1.44	Si5	1.44	Si5	1.46
Si6	1.47	Si6	1.46	Si6	1.46	Si6	1.46	Si6	1.46	Si6	1.44
O7	–0.72	O7	–0.72	O7	–0.72	O7	–0.72	O7	–0.72	O7	–0.66
O8	–0.83	O8	–0.83	O8	–0.83	O8	–0.83	O8	–0.83	O8	–0.83
O9	–0.78	O9	–0.78	O9	–0.78	O9	–0.78	O9	–0.78	O9	–0.78
O10	–1.00	O10	–0.99	O10	–1.00	O10	–0.99	O10	–1.05	O10	–1.06
O11	–0.81	O11	–0.81	O11	–0.81	O11	–0.81	O11	–0.81	O11	–0.80
O12	–0.95	O12	–0.95	O12	–0.96	O12	–0.96	O12	–0.98	O12	–0.96
Si13	1.41	Si13	1.41	Si13	1.38	Si13	1.39	Si13	1.36	Si13	1.35
O14	–0.76	O14	–0.76	O14	–0.76	O14	–0.77	O14	–0.77	O14	–0.72
O15	–0.69	O15	–0.69	O15	–0.70	O15	–0.70	O15	–0.70	O15	–0.78
Sn16	1.69	Sn16	1.70	Sn16	1.71	Sn16	1.71	Sn16	1.69	Sn16	1.69
O17	–0.81	O17	–0.81	O17	–0.81	O17	–0.81	O17	–0.80	O17	–0.80
O18	–0.88	O18	–0.88	O18	–0.88	O18	–0.88	O18	–0.88	O18	–0.88
Sn19	1.69	Sn19	1.69	Sn19	1.70	Sn19	1.69	Sn19	1.69	Sn19	1.69
Sn20	1.66	Sn20	1.66	Sn20	1.66	Sn20	1.66	Sn20	1.65	Sn20	1.65
Sn21	1.69	Sn21	1.69	Sn21	1.69	Sn21	1.69	Sn21	1.70	Sn21	1.69
O22	–0.84	O22	–0.84	O22	–0.84	O22	–0.84	O22	–0.84	O22	–0.84
O23	–0.89	O23	–0.89	O23	–0.89	O23	–0.89	O23	–0.89	O23	–0.88
O24	–1.04	O24	–1.04	O24	–1.06	O24	–1.06	O24	–1.11	O24	–1.11
O25	–0.90	O25	–0.90	O25	–0.90	O25	–0.90	O25	–0.90	O25	–0.90
O26	–1.00	O26	–1.00	O26	–1.03	O26	–1.02	O26	–1.06	O26	–1.06
O27	–0.94	O27	–0.94	O27	–0.93	O27	–0.93	O27	–0.92	O27	–0.92
Sn28	1.78	Sn28	1.78	Sn28	1.82	Sn28	1.83	Sn28	1.68	Sn28	1.69
O29	–0.88	O29	–0.88	O29	–0.90	O29	–0.89	O29	–0.89	O29	–0.89
O30	–0.86	O30	–0.86	O30	–0.86	O30	–0.86	O30	–0.86	O30	–0.86
Li31	0.70	Li31	0.60	Na31	0.78	Na31	0.69	K31	0.89	K31	0.84
Li32	0.68	Li32	0.58	Na32	0.66	Na32	0.57	K32	0.87	K32	0.86
–	–	H33	–0.02	–	–	H33	–0.02	–	–	H33	–0.05
–	–	H34	–0.00	–	–	H34	–0.01	–	–	H34	–0.04
–	–	H35	0.12	–	–	H35	0.09	–	–	H35	0.08
–	–	H36	0.10	–	–	H36	0.08	–	–	H36	0.06

ing lithium, sodium and potassium, the negative atomic charge of oxygen atoms of O2, O3, O7–O12, O14, O15, O17, O18, O22–O27, O29, O30 in Li_2[SnO–SiO]–$2H_2$, Na_2[SnO–SiO]–$2H_2$ or K_2[SnO–SiO]–$2H_2$ nanoclusters augments. In fact, Li_2[SnO–SiO], Na_2[SnO–SiO] or K_2[SnO–SiO] nanoclusters have shown more efficiency than [SnO–SiO] cluster [30] for admitting the electron from electron donor of H33, H34, H35 and H36 (Table 1 and Figs. 3a–3c).

The changes of charge density analysis in the adsorption process have illustrated that Li_2 [SnO–

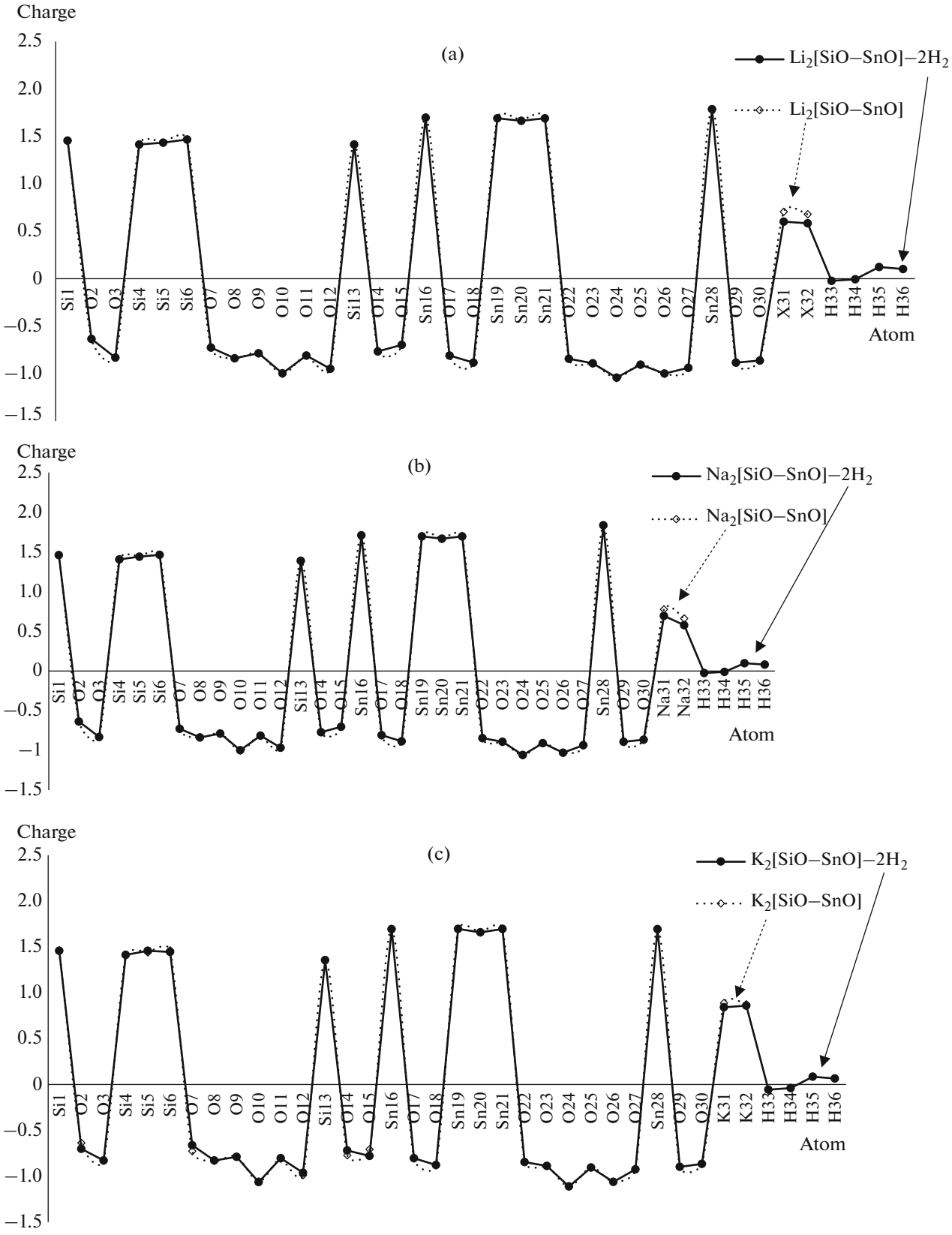

Fig. 3. The fluctuation of atomic charge (Q/coulomb) for (a) $Li_2[SnO–SiO]$, (b) $Na_2[SnO–SiO]$ or (c) $K_2[SnO–SiO]$ nanoclusters.

SiO] has shown the "Bader charge" of −1.631 coulomb before hydrogen adsorption and −1.633 coulomb after hydrogen adsorption. Moreover, the changes of charge density analysis for Na_2[SnO–SiO] has shown the "Bader charge" of −1.626 coulomb before hydrogen adsorption and −1.635 coulomb after hydrogen adsorption. However, K_2[SnO–SiO] has shown the "Bader charge" of −1.574 coulomb before hydrogen adsorption and after hydrogen adsorption. The differences of charge density for these structures are measured as: $\Delta Q_{Li_2[SnO-SiO]} = -0.002$, $\Delta Q_{Na_2[SnO-SiO]} = -0.009$ and $\Delta Q_{K_2[SnO-SiO]} = 0$. Therefore, the results have shown that the cluster of Na_2[SnO–SiO] and Li_2 [SnO–SiO] may have the most tensity for electron accepting owing to hydrogen grabbing.

3.2. TDOS Analysis

Squirming the molecular orbital data owing to gaussian graphs of unit altitude and entire width at "half maximum (FWHM)" of 0.3 eV by "GaussSum 3.0.2" [65] have computed total density of states (TDOS) diagrams. Regarding adsorption behavior of hydrogen by Li_2[SnO–SiO], Na_2[SnO–SiO] or K_2[SnO–SiO] nanoclusters, TDOS has been measured. This parameter can indicate the existence of important chemical interactions often on the convex side (Figs. 4a, 4a', 4b, 4b', 4c, 4c'). During formation of Li_2[SnO–SiO] cluster, Fig. 4a has shown the peaks with the highest intensity around −0.3, −0.45 and −0.60 a.u. due to covalent bond between two atoms of Li_2 with [SnO–SiO] cluster. Moreover, Li_2[SnO–SiO]–$2H_2$ has indicated a duplicate peak around −0.45 to −0.5 a.u. during hydrogen adsorption (Fig. 4a'). After H-grabbing by Na_2[SnO–SiO] cluster, pointed peaks around −0.3, −0.45 and −0.60 a.u. due to covalent bond between two atoms of Na with [SnO–SiO] cluster (Fig. 4b). Furthermore, Na_2[SnO–SiO]–$2H_2$ has indicated a duplicate peak around −0.45 to −0.5 a.u. during hydrogen adsorption (Fig. 4b'). However, the maximum energy of TDOS for K_2[SnO–SiO] (Fig. 4c) with several peaks around −0.35, −0.45, −0.6 and −0.75 a.u. with maximum density of state of ≈23 around −0.35 a.u. has been shown. Moreover, similar amounts of TDOS for K_2[SnO–SiO]–$2H_2$ (Fig. 4c') through some fluctuations in the behavior of the graphs have been observed.

3.3. ELF Analysis

A type of scalar fields called electron localization function (ELF) may demonstrate a broad span of bonding samples. Nevertheless, the distinction between deduced/raised electron delocalization/localization into cyclic π-conjugated sets stays encouraging for ELF [66]. The grosser the electron localization is in an area, the more likely the electron movement is restricted within it. Therefore, they might be discerned from the ones away if electrons are totally centralized. As Bader investigated, the zones with large electron localization possess extensive magnitudes of Fermi hole integration [67]. But, with having a six-dimension function for the Fermi hole, it seems hard to be studied directly. Then, Becke and Edgecombe remarked that spherically averaged like spin conditional pair probability possesses a direct correlation with the Fermi hole and proposed the parameter of ELF in Multiwfn program [68, 69] and popularized for spin-polarized procedure [70]:

$$\mathrm{ELF}(r) = \frac{1}{1 + [D(r)/D_0(r)]}, \quad (1)$$

where

$$D(r) = \frac{1}{2}\sum_i \eta_i |\nabla\varphi_i(r)|^2 - \frac{1}{8}\left[\frac{|\nabla\rho_\alpha(r)|^2}{\rho_\alpha(r)} + \frac{|\nabla\rho_\beta(r)|^2}{\rho_\beta(r)}\right], \quad (2)$$

and

$$D_0(r) = \frac{3}{10}\left(6\pi^2\right)^{2/3}\left[\rho_\alpha(r)^{5/3} + \rho_\beta(r)^{5/3}\right]. \quad (3)$$

For close-shell system, since $\rho_\alpha = \rho_\beta = (1/2)\rho$, D and D_0 terms can be simplified as:

$$D(r) = \frac{1}{2}\sum_i \eta_i |\nabla\varphi_i(r)|^2 - \frac{1}{8}\frac{|\nabla\rho(r)|^2}{\rho(r)}, \quad (4)$$

and

$$D_0(r) = (3/10)\left(3\pi^2\right)^{2/3}\rho(r)^{5/3}. \quad (5)$$

Regarding kinetic energy, ELF was rechecked to be more punctual for both Kohn–Sham DFT and post-HF wavefunctions [71]. In fact, the excess kinetic energy density caused by Pauli repulsion was unfolded by $D(r)$ and $D_0(r)$ may be inspected as Thomas–Fermi kinetic energy density. Because $D_0(r)$ is brough forward the ELF as origin, what the ELF shows is an affiliate localization. Trapping of hydrogens by Li_2[SnO–SiO], Na_2[SnO–SiO] or K_2[SnO–SiO] nanoclusters towards formation of Li_2[SnO–SiO]–$2H_2$, Na_2[SnO–SiO]–$2H_2$ or K_2[SnO–SiO]–$2H_2$ can be defined by ELF graphs owing to exploring their delocalization/localization characterizations of electrons and chemical bonds (Figs. 5a, 5a', 5b, 5b', 5c, 5c').

A vaster jointed area engaged by an isosurface map has shown the electron delocalization in Li_2[SnO–SiO] (Fig. 5a), Li_2[SnO–SiO] –$2H_2$ (Fig. 5a'), Na_2[SnO–SiO] (Fig. 5b), Na_2 [SnO–SiO]–$2H_2$ (Fig. 5b'), K_2 [SnO–SiO] (Fig. 5c), and K_2[SnO–SiO]–$2H_2$ (Fig. 5c') through labeling atoms of O12, Si13, O26, Ge28, X31(X = Li, Na or K) and H35. In fact, the counter map of ELF can confirm that Li_2[SnO–SiO], Na_2[SnO–SiO], or K_2[SnO–SiO] nanocluster may increase the efficiency during hydro-

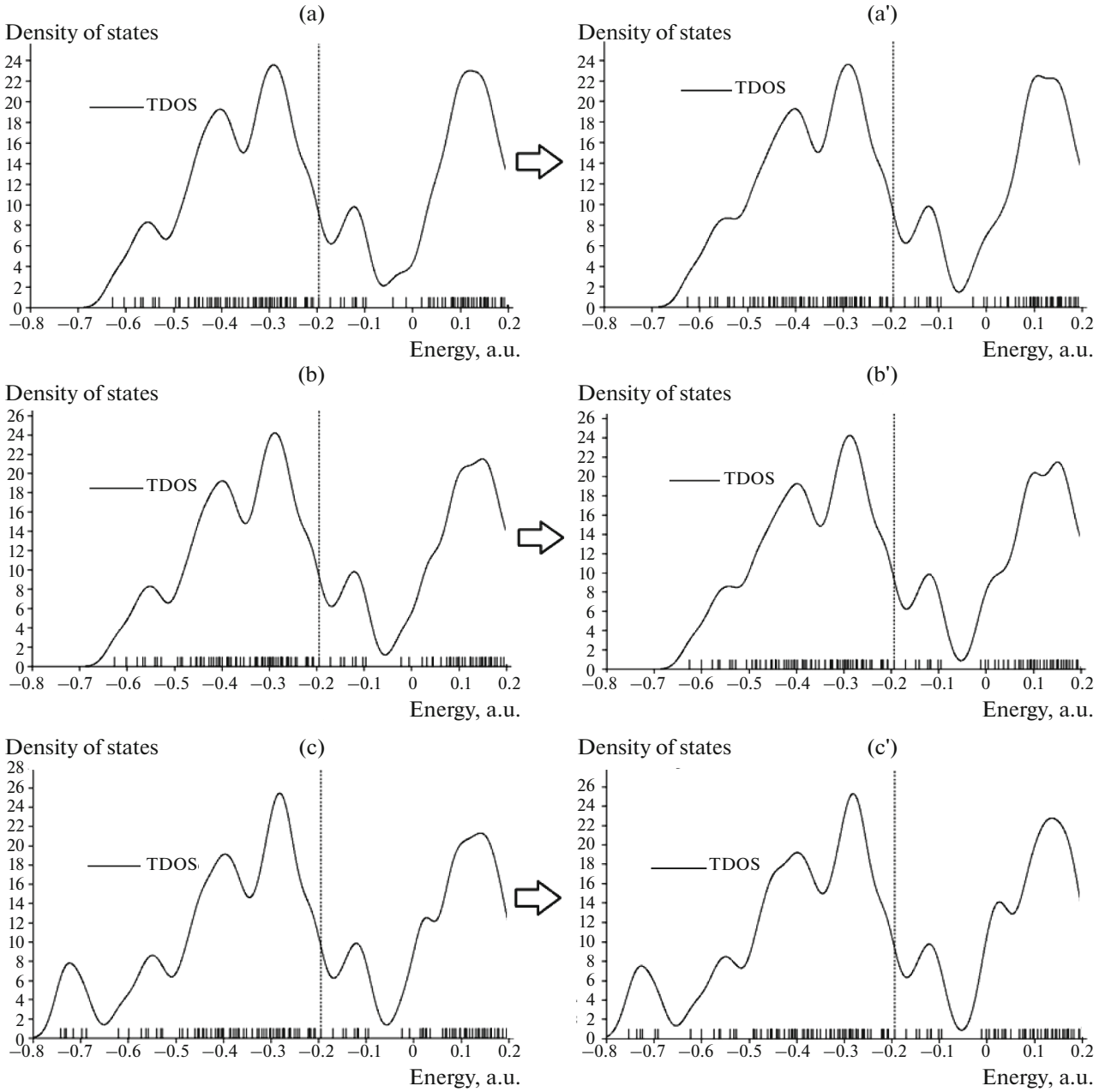

Fig. 4. TDOS graphs of (a) Li_2[SnO–SiO], (a') Li_2[SnO–SiO]–$2H_2$, (b) Na_2[SnO–SiO], (b') Na_2[SnO–SiO]–$2H_2$, (c) K_2[SnO–SiO], and (c') K_2[SnO–SiO]–$2H_2$ nanoclusters.

gen adsorption towards formation of Li_2[SnO–SiO]–$2H_2$, Na_2 [SnO–SiO]–$2H_2$, or K_2 [SnO–SiO]–$2H_2$ nanocluster.

Moreover, intermolecular orbital overlap integral is important in discussions of intermolecular charge transfer which can calculate HOMO-HOMO and LUMO-LUMO overlap integrals between the H_2 molecules and heteroclusters of Li_2[SnO–SiO], Na_2[SnO–SiO] or K_2[SnO–SiO]. The applied wavefunction level is CAM–B3LYP–D3/6–311+G(*d*,*p*) that corresponds to HOMO and LUMO, respectively (Table 2).

The amount of "Mayer bond order" [72] is generally according to empirical bond order for the single bond is near 1.0. "Mulliken bond order" [73] with a small accord with empirical bond order is not appropriate for quantifying bonding strength, for which Mayer bond order always performs better. However, "Mulliken bond order" is a good qualitative indicator for "positive amount" of bonding and "negative

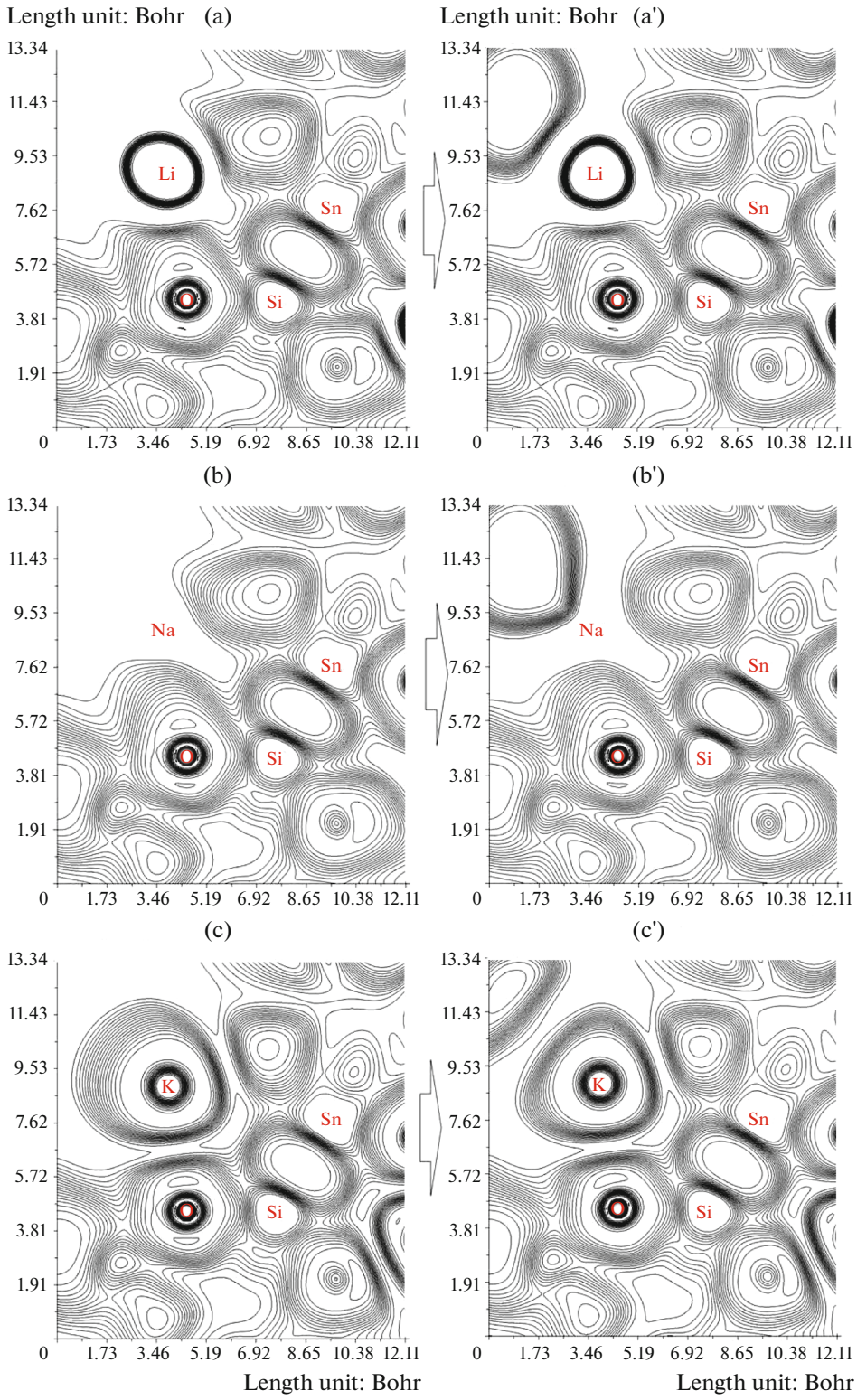

Fig. 5. The counter map of ELF graphs for (a) $Li_2[SnO–SiO]$, (a') $Li_2[SnO–SiO]–2H_2$, (b) $Na_2[SnO–SiO]$, (b') $Na_2[SnO–SiO]–2H_2$, (c) $K_2[SnO–SiO]$, and (c') $K_2[SnO–SiO]–2H_2$ nanoclusters.

Table 2. LUMO, HOMO, energy gap (ΔE), Ring perimeter (Å), Total ring area (Å^2) for Li_2[SnO–SiO], Na_2[SnO–SiO], K_2[SnO–SiO] through hydrogen grabbing and formation of Li_2[SnO–SiO]–$2H_2$, Na_2[SnO–SiO]–$2H_2$, K_2[SnO–SiO]–$2H_2$ heteroclusters

Heteroclusters	Dipole moment, D	E_{HOMO}, eV	E_{LUMO}, eV	$\Delta E = E_{LUMO} - E_{HOMO}$, eV	Ring perimeter, Å	Total ring area, Å^2
Li_2[SnO–SiO]	5.18	–5.36	–4.70	0.6512	9.33	5.15
Na_2[SnO–SiO]	5.133	–5.31	–4.65	0.6600	9.91	6.67
K_2[SnO–SiO]	5.10	–5.31	–4.62	0.6862	9.91	6.67
Li_2[SnO–SiO]–$2H_2$	5.24	–5.31	–4.66	0.6507	9.91	6.67
Na_2[SnO–SiO]–$2H_2$	5.17	–5.29	–4.63	0.6596	9.91	6.67
K_2[SnO–SiO]–$2H_2$	4.89	–5.29	–4.64	0.6525	9.91	6.67

Table 3. The bond order of Mayer, Wiberg, Mulliken, Laplacian and Fuzzy from mixed alpha and beta density matrix for Li_2[SnO–SiO], Na_2[SnO–SiO], K_2[SnO–SiO] heteroclusters

Compound	Bond type	Bond order				
		mayer	wiberg	mulliken	laplacian	fuzzy
Li_2[SnO–SiO]	O12–Si13	0.47	0.60	0.14	0.20	1.00
	O12–Li31	0.15	0.21	0.14	0.23	0.13
	O26–Sn28	0.44	0.53	0.23	0.46	1.20
	O26–Li31	0.25	0.28	0.20	0.16	0.15
Na_2[SnO–SiO]	O12–Si13	0.49	0.60	0.18	0.19	0.96
	O12–Na31	0.11	0.16	0.11	0.14	0.31
	O26–Sn28	0.43	0.53	0.23	0.43	1.15
	O26–Na31	0.19	0.20	0.16	0.14	0.33
K_2[SnO–SiO]	O12–Si13	0.51	0.61	0.20	0.18	0.96
	O12–K31	0.23	0.14	0.07	0.18	0.36
	O26–Sn28	0.49	0.54	0.29	0.41	1.14
	O26–K31	0.06	0.18	0.15	0.14	0.39

amount" of antibonding which are evacuated and localized, respectively (Tables 3, 4).

As it is seen in Tables 3, 4, "Laplacian bond order" [74] has a straight cohesion with bond polarity, bond dissociation energy and bond vibrational frequency. The low value of Laplacian bond order might demonstrate that it is insensitive to the calculation degree applied for producing electron density. Generally, the value of "Fuzzy bond order" is near Mayer bond order, especially for low-polar bonds, but much more stable with respect to the change in basis-set. Computation of "Fuzzy bond order" demands running "Becke's DFT" numerical integration, owing to which the calculation value is larger than assessment of "Mayer bond order" and it can concede more precisely [75, 76]. Newly, the research on Na/K-atom devices has grown rapidly to reach the goals of practical applications. One of the current priorities is the optimization of electrolytes from the aspects of scientific issues, including structure improvement, formula

Table 4. The bond order of Mayer, Wiberg, Mulliken, Laplacian and Fuzzy from mixed alpha and beta density matrix for hydrogenated heteroclusters of $Li_2[SnO–SiO]–2H_2$, $Na_2[SnO–SiO]–2H_2$, $K_2[SnO–SiO]–2H_2$

Compound	Bond type	Bond order				
		mayer	wiberg	mulliken	laplacian	fuzzy
$Li_2[SnO–SiO]–2H_2$	O12–Si13	0.47	0.60	0.14	0.20	1.00
	O12–Li31	0.16	0.21	0.15	0.19	0.13
	O26–Sn28	0.43	0.53	0.23	0.46	1.20
	O26–Li31	0.25	0.28	0.21	0.30	0.15
	Li31–H33	0.10	0.18	0.09	0.08	0.20
$Na_2[SnO–SiO]–2H_2$	O12–Si13	0.48	0.60	0.18	0.19	0.96
	O12–Na31	0.12	0.16	0.12	0.13	0.31
	O26–Sn28	0.42	0.53	0.23	0.43	1.15
	O26–Na31	0.20	0.20	0.17	0.16	0.33
	Na31–H33	0.08	0.16	0.07	0.06	0.20
$K_2[SnO–SiO]–2H_2$	O12–Si13	0.51	0.62	0.20	0.20	0.97
	O12–K31	0.17	0.13	0.06	0.10	0.35
	O26–Sn28	0.48	0.54	0.28	0.41	1.14
	O26–K31	0.11	0.18	0.14	0.10	0.39
	K31–H33	0.06	0.17	0.05	0.04	0.20

adjustment involving variety and concentration of salts and solvents.

CONCLUSIONS

In this article, we have expounded the advanced analysis and characterization technology of electrolytes, and applications of Na/K devices. In summary, H-grabbing by the nanoclusters of $Li_2[SnO–SiO]$, $Na_2[SnO–SiO]$ or $K_2[SnO–SiO]$ was investigated by first-principles computations of DFT method. The alterations of charge density illustrated a remarkable charge transfer towards $Li_2[SnO–SiO]$, $Na_2[SnO–SiO]$ or $K_2[SnO–SiO]$. The fluctuation in charge density values demonstrates that the electronic densities were in the boundary of adsorbate/adsorbent atoms during the adsorption status. Besides, thermodynamic parameters describing H-grabbing by alkali metals-based nanoclusters of $Li_2[SnO–SiO]$, $Na_2[SnO–SiO]$ or $K_2[SnO–SiO]$ have been investigated including internal process of the adsorbent–adsorbate system.

It is well established that the addition of Li, Na or K to cell batteries may increase the energy storage in cell batteries. In this work, we explore the effect of Li, Na or K on [SnO–SiO] heterocluster. Moreover, hydrogen bond (H-bond) accepting sites by $Li_2[SnO–SiO]$, $Na_2[SnO–SiO]$ or $K_2[SnO–SiO]$ can alleviate parasitic hydrogen evolution in aqueous electrolytes in lithium, sodium, or potassium-ion batteries. Today, it is crucial to distinguish the potential of hydrogen technologies and bring up all perspectives of their performance, from technological progresses to economic and social effects. The authors intend to pursue research on sustainability and clean energy subjects towards finding new solutions for reducing the global dependency on fossil fuels. Finally, it is proposed the perspective on current dilemmas and outlook future direction of electrolytes in the post lithium era. Na/K devices will be hopeful options to replace LIBs due to their similar characteristics and cheap cost, but numerous research and efforts on electrolytes should be focused on optimizing the performance of devices

and popularize their practical application in the future.

ACKNOWLEDGMENTS

In successfully completing this paper and its research, the authors are grateful to Kastamonu University.

FUNDING

This work was supported by ongoing institutional funding. No additional grants to carry out or direct this particular research were obtained.

CONFLICT OF INTEREST

The authors of this work declare that they have no conflicts of interest.

REFERENCES

1. E. N. Antonov, A. G. Ivanova, L. I. Krotova, et al., Russ. J. Phys. Chem. B **17**, 1555–1560 (2023). https://doi.org/10.1134/S199079312308002X
2. F. Mollaamin, Russ. J. Phys. Chem. B **18**, 805–820 (2024). https://doi.org/10.1134/S1990793124700131
3. M. Monajjemi, M. T. Baie, and F. Mollaamin, Russ. Chem. Bull. **59**, 886–889 (2010). https://doi.org/10.1007/s11172-010-0181-5
4. F. Mollaamin, S. Mohammadi, Z. Khalaj, et al., Russ. J. Phys. Chem. B **18**, 67–82 (2024). https://doi.org/10.1134/S1990793124010330
5. V. Y. Agroskin, B. G. Bravy, G. K.Vasiliev, et al., Russ. J. Phys. Chem. B **17**, 1265–1269 (2023). https://doi.org/10.1134/S1990793123060131
6. A. Tahan, F. Mollaamin, and M. Monajjemi, Russ. J. Phys. Chem. A **83**, 587–597 (2009). https://doi.org/10.1134/S003602440904013X
7. S. Shahriari, M. Monajjemi, F. Mollaamin, J. Chil. Chem. Soc. **67**, 5468–5476 (2022). https://doi.org/10.4067/S0717-97072022000205468
8. A. M. Tereza, G. L. Agafonov, E. K. Anderzhanov, et al., Russ. J. Phys. Chem. B **17**, 1294–1299 (2023). https://doi.org/10.1134/S1990793123060246
9. V. I. Petinov, V. M. Timin, K. V. Bozhenko, et al., Russ. J. Phys. Chem. B **18**, 365–368 (2024). https://doi.org/10.1134/S1990793124020301
10. A. M. Tereza, G. L. Agafonov, E. K. Anderzhanov, et al., Russ. J. Phys. Chem. B **17**, 974–978 (2023). https://doi.org/10.1134/S1990793123040309
11. M. A. A. Zadeh, H. Lari, L. Kharghanian, et al., J. Comput. Theor. Nanosci. **12**, 4358 (2015). https://doi.org/10.1166/jctn.2015.4366
12. E. I. Rudenko, N. V. Dohlikova, A. K.Gatin, et al., Russ. J. Phys. Chem. B **17**, 845–852 (2023). https://doi.org/10.1134/S1990793123040164
13. E. M. Sarasia, S. Afsharnezhad, B. Honarparvar, et al., Phys. Chem. Liq. **49**, 561–571(2011). https://doi.org/10.1080/00319101003698992
14. M. Monajjemi, H. Yamola, and F. Mollaamin, Fuller. Nanotub. Carbon Nanostruct. **22**, 595–603 (2014). https://doi.org/10.1080/1536383X.2012.702163
15. F. Mollaamin, F. Najafi, M. Khaleghian, B. Khalili Hadad, and M. Monajjemi, Fulleren Nanotubes Carbon Nanostruct. **19**, 653–667 (2011). https://doi.org/10.1080/1536383X.2010.504956
16. S. Shahriari, M. Monajjemi, and K. Zare, Biointerface Res. Appl. Chem. **8**, 3219–3223 (2018).
17. R. R. Kayumov, A. P. Radaeva, A. A. Krupina, et al., Russ. J. Phys. Chem. B **17**, 801–809 (2023). https://doi.org/10.1134/S1990793123040097
18. M. Khaleghian, M. Zahmatkesh, F. Mollaamin, et al., Fulleren Nanotubes Carbon Nanostruct. 19, 251–261 (2011). https://doi.org/10.1080/15363831003721757
19. K. Y. Troshin, N. M. Rubtsov, G. I. Tsvetkov, et al., Russ. J. Phys. Chem. B **17**, 979–985 (2023). https://doi.org/10.1134/S1990793123040310
20. K. Y. Troshin, N. M. Rubtsov, G. I. Tsvetkov, et al., Russ. J. Phys. Chem. B **17**, 433–438 (2023). https://doi.org/10.1134/S1990793123020185
21. Q. Q. Xiong, Russ. J. Phys. Chem. B **18**, 638–644 (2024). https://doi.org/10.1134/S1990793124700155
22. F. Mollaamin and M. Monajjemi, J. Comput. Theor. Nanosci. **12**, 1030–1039 (2015). https://doi.org/10.1166/jctn.2015.3846
23. X. Yuan, X. Tan, and B. Liu, Russ. J. Phys. Chem. B **17**, 886–895 (2023). https://doi.org/10.1134/S1990793123040322
24. L. I. Trakhtenberg, Russ. J. Phys. Chem. B **17**, 600–607 (2023). https://doi.org/10.1134/S1990793123030144
25. K. Bakhshi, F. Mollaamin, and M. Monajjemi, J. Comput. Theor. Nanosci. **8**, 763–768 (2011). https://doi.org/10.1166/jctn.2011.1750
26. F. Mollaamin, M. Monajjemi, S. Salemi, et al., Fulleren Nanotubes Carbon Nanostruct. **19**, 182 (2011). https://doi.org/10.1080/15363831003782932
27. M. Monajjemi, M. Khaleghian, N. Tadayonpour, et al., Int. J. Nanosci. **09**, 517–529 (2010). https://doi.org/10.1142/S0219581X10007071
28. F. Mollaamin and M. Monajjemi, J. Cluster Sci. **34**, 2901–2918 (2023). https://doi.org/10.1007/s10876-023-02436-5
29. N. Yodsin, H. Sakagami, T. Udagawa, et al., Mol. Catal. **504**, 111486 (2021). https://doi.org/10.1016/j.mcat.2021.111486
30. A. E. Galashev, Russ. J. Phys. Chem. B **17**, 113–121 (2023). https://doi.org/10.1134/S1990793123010190
31. T. Wei, Y. Zhou, C. Sun, et al., Nano Res. **17**, 2763–2769 (2024). https://doi.org/10.1007/s12274-023-6187-8
32. K. Yao, M. Ling, G. Liu, et al., J. Phys. Chem. Lett. **9**, 5130–5134 (2018). https://doi.org/10.1021/acs.jpclett.8b02066
33. U. Cardella, L. Decker, J. Sundberg, et al., Int. J. Hydrogen Energy **42**, 12339–12354 (2017). https://doi.org/10.1016/j.ijhydene.2017.03.167

34. A. Hammad and I. Dincer, Int. J. Hydrogen Energy **43**, 1139–1151 (2018). https://doi.org/10.1016/j.ijhydene.2017.10.158

35. O. A. Kim, T. V. Bogdan, A. E. Koklin, et al., Russ. J. Phys. Chem. B **16**, 1218–1220 (2022). https://doi.org/10.1134/S1990793122070107

36. M. A. Qyyum, Y. D. Chaniago, W. Ali, et al., Energies **13**, 5023 (2020). https://doi.org/10.3390/en13195023

37. A. H. Davtyan, Z. H. Manukyan, S. D. Arsentev, et al. Russ. J. Phys. Chem. B **18**, 461–467 (2024). https://doi.org/10.1134/S1990793124020209

38. X. Yu, X. Zhang, H. Wang, et al., J. Phys. Chem. C **121**, 22081–22091 (2017). https://doi.org/10.1021/acs.jpcc.7b06361

39. F. Mollaamin and M. Monajjemi, J. Mol. Model. **29**, 119 (2023). https://doi.org/10.1007/s00894-023-05526-3

40. E. Rivard, M. Trudeau, and K. Zaghib, Materials **12**, 1973 (2019). https://doi.org/10.3390/ma12121973

41. F. Mollaamin and M. Monajjemi, Russ. J. Phys. Chem. B **17**, 658–672 (2023). https://doi.org/10.1134/S1990793123030223

42. F. Mollaamin and M. Monajjemi, Russ. J. Phys. Chem. B **18**, 607–623 (2024). https://doi.org/10.1134/S1990793124020271

43. F. Mollaamin, S. Shahriari, and M. Monajjemi, Russ. J. Phys. Chem. B **18**, 398–418 (2024). https://doi.org/10.1134/S199079312402026X

44. V. Y. Agroskin, B. G. Bravy, G. K.Vasiliev, et al., Russ. J. Phys. Chem. B **16**, 596–601 (2022). https://doi.org/10.1134/S1990793122040029

45. T. Yanai, D. P. Tew, and N. C. Handy, Chem. Phys. Lett. **393**, 51–57 (2004). https://doi.org/10.1016/j.cplett.2004.06.011

46. G. Henkelman, A. Arnaldsson, and H. Jónsson, Comput. Mater. Sci. **36**, 354–360 (2006). https://doi.org/10.1016/j.commatsci.2005.04.010

47. R. F. Bader, *Atoms in Molecules: A Quantum Theory* (Oxford Univ. Press, Oxford, 1990)

48. F. Mollaamin and M. Monajjemi, Russ. J. Phys. Chem. B **18**, 533–548 (2024). https://doi.org/10.1134/S199079312402012X

49. B. Khalili Hadad, F. Mollaamin, and M. Monajjemi, Russ. Chem. Bull. **60**, 238–241 (2011). https://doi.org/10.1007/s11172-011-0039-5

50. F. Mollaamin, S. Mohammadi, Z. Khalaj, et al., Russ. J. Phys. Chem. B **18**, 67–82 (2024). https://doi.org/10.1134/S1990793124010330

51. M. Monajjemi, F. Mollaamin, and S. Shojaei, Biointerface Res. Appl. Chem. **10**, 5575 (2020). https://doi.org/10.33263/BRIAC103.575585

52. F. Mollaamin and M. Monajjemi, Comput. Theor. Chem. **1237**, 114666 (2024). https://doi.org/10.1016/j.comptc.2024.114666

53. S. Shahriari, F. Mollaamin, and M. Monajjemi, Micromachines **14**, 241 (2023). https://doi.org/10.3390/mi14020241

54. F. Mollaamin and M. Monajjemi, J. Mol. Struct. **1300**, 137214 (2024). https://doi.org/10.1016/j.molstruc.2023.137214

55. F. Mollaamin, A. Ilkhani, N. Sakhaei, et al., J. Comput. Theor. Nanosci. **12**, 3148–3154 (2015). https://doi.org/10.1166/jctn.2015.4092

56. F. Mollaamin and M. Monajjemi, Sensor Rev. **44**, 179–193 (2024). https://doi.org/10.1108/SR-01-2024-0066

57. M. Monajjemi, L. Mahdavian, F. Mollaamin, et al., Russ. J. Inorg. Chem. **54**, 1465–1473 (2009). https://doi.org/10.1134/S0036023609090216

58. F. Mollaamin and M. Monajjemi, Russ. J. Phys. Chem. B **18**, 49–66 (2024). https://doi.org/10.1134/S1990793124010159

59. F. Mollaamin and M. Monajjemi, Int. J. Quantum Chem. **124**, e27348 (2024). https://doi.org/10.1002/qua.27348

60. F. Mollaamin and M. Monajjemi, Mol. Simul. **49**, 365–376 (2023). https://doi.org/10.1080/08927022.2022.2159996

61. S. V. Feskov, Russ. J. Phys. Chem. B **18**, 1–8 (2024). https://doi.org/10.1134/S1990793124010081

62. M. J. Frisch, G. W. Trucks, H. B. Schlegel, G. E. Scuseria, M. A. Robb, J. R. Cheeseman, G. Scalmani, V. Barone, G. A. Petersson, H. Nakatsuji, X. Li, M. Caricato, A. V. Marenich, J. Bloino, B. G. Janesko, R. Gomperts, B. Mennucci, H. P. Hratchian, J. V. Ortiz, A. F. Izmaylov, J. L. Sonnenberg, D. Williams-Young, F. Ding, F. Lipparini, F. Egidi, J. Goings, B. Peng, A. Petrone, T. Henderson, D. Ranasinghe, V. G. Zakrzewski, J. Gao, N. Rega, G. Zheng, W. Liang, M. Hada, M. Ehara, K. Toyota, R. Fukuda, J. Hasegawa, M. Ishida, T. Nakajima, Y. Honda, O. Kitao, H. Nakai, T. Vreven, K. Throssell, J. A. Montgomery, Jr., J. E. Peralta, F. Ogliaro, M. J. Bearpark, J. J. Heyd, E. N. Brothers, K. N. Kudin, V. N. Staroverov, T. A. Keith, R. Kobayashi, J. Normand, K. Raghavachari, A. P. Rendell, J. C. Burant, S. S. Iyengar, J. Tomasi, M. Cossi, J. M. Millam, M. Klene, C. Adamo, R. Cammi, J. W. Ochterski, R. L. Martin, K. Morokuma, O. Farkas, J. B. Foresman, and D. J. Fox, *Gaussian 16, Revision C.01* (Gaussian, Inc., Wallingford, CT, 2016).

63. R. Dennington, T. A. Keith, and J. M. Millam, *GaussView, Version 6.06.16* (Semichem Inc., Shawnee Mission, KS, 2016).

64. Z. Xu, C. Qin, Y. Yu, et al., AIP Adv. **14**, 055114 (2024). https://doi.org/10.1063/5.0208082

65. N. M. O'Boyle, A. L. Tenderholt, and K. M. Langner. J. Comp. Chem. **29**, 839–845 (2008). https://doi.org/10.1002/jcc.20823

66. C. F. Matta, P. W. Ayers, and R. Cook, "The physics of electron localization and delocalization, in *Electron Localization-Delocalization Matrices*, Lecture Notes in Chemistry, (Springer, Cham, 2024). https://doi.org/10.1007/978-3-031-51434-0_2

67. R. F. W. Bader, Theor. Chem. Acc. **105**, 276–283 (2001). https://doi.org/10.1007/s002140000233

68. T. Lu and F. Chen, J. Comput. Chem. **33**, 580–592 (2012). https://doi.org/10.1002/jcc.22885
69. T. Lu, J. Chem. Phys. **161**, 082503 (2024). https://doi.org/10.1063/5.0216272
70. A. D. Becke and K. E. Edgecombe, J. Chem. Phys. **92**, 5397–5403 (1990). . https://doi.org/10.1063/1.458517
71. A. Savin, O. Jepsen, J. Flad, et al., Angew. Chem. Int. Ed. **31**, 187–188 (1992). https://doi.org/10.1002/anie.199201871
72. I. Mayer, Chem. Phys. Lett. **544**, 83–86 (2012). https://doi.org/10.1016/j.cplett.2012.07.0
73. F. Mollaamin, M. T. Baei, M. Monajjemi, et al., Russ. J. Phys. Chem. **82**, 2354–2361 (2008). https://doi.org/10.1134/S0036024408130323
74. T. Lu and F. Chen, J. Phys. Chem. A **117**, 3100–3108 (2013). https://doi.org/10.1021/jp4010345
75. X. Wang, X. Zhang, W. Pedrycz, et al., Fractal Fract. **8**, 523 (2024). https://doi.org/10.3390/fractalfract8090523
76. F. Mollaamin and M. Monajjemi, Energy Storage **7**, e70122 (2025). https://doi.org/10.1002/est2.70122